

The ${}^3\text{He}(\vec{n}, p){}^3\text{H}$ parity-conserving asymmetry

M. Viviani^{1*}, S. Baeßler^{2,3}, L. Barrón-Palos⁴, N. Birge^{5,6}, J.D. Bowman³, J. Calarco⁷, V. Cianciolo³, C.E. Coppola⁵, C.B. Crawford⁸, G. Dodson⁹, N. Fomin⁵, I. Garishvili^{3,5}, M.T. Gericke¹⁰, L. Girlanda^{11,12}, G.L. Greene^{5,3}, G.M. Hale⁶, J. Hamblen¹³, C. Hayes^{5,14}, E. B. Iverson³, M.L. Kabir^{8,15}, A. Kievsky¹, L.E. Marcucci^{16,1}, M. McCrea^{10,17}, E. Plemons⁵, A. Ramírez-Morales⁴, P.E. Mueller³, I. Novikov¹⁸, S.I. Penttilä³, E.M. Scott^{5,19}, J. Watts¹³, and C. Wickersham¹³

¹ *Istituto Nazionale di Fisica Nucleare,
Sezione di Pisa, I-56127 Pisa, Italy*

² *University of Virginia,
Charlottesville, Virginia 22904, USA*

³ *Oak Ridge National Laboratory,
Oak Ridge, Tennessee 37830, USA*

⁴ *Instituto de Física,
Universidad Nacional Autónoma de México,
Apartado Postal 20-364, 01000, México*

⁵ *University of Tennessee Knoxville,
Knoxville, Tennessee 37996, USA*

⁶ *Los Alamos National Laboratory,
Los Alamos, New Mexico 87545, USA*

⁷ *University of New Hampshire,
Durham, New Hampshire 03824, USA*

⁸ *University of Kentucky,
Lexington, Kentucky 40506, USA*

⁹ *Massachusetts Institute of Technology,
Cambridge, Massachusetts 02139, USA*

¹⁰ *University of Manitoba, Manitoba R3T 2N2, Canada*

¹¹ *Department of Mathematics and Physics,
University of Salento, I-73100 Lecce, Italy*

¹² *Istituto Nazionale di Fisica Nucleare,
Sezione di Lecce, I-73100 Lecce, Italy*

¹³ *University of Tennessee Chattanooga,
Chattanooga, Tennessee 37403, USA*

¹⁴ *Indiana University, Bloomington, Indiana 47405, USA*

¹⁵ *Brookhaven National Laboratory,
Upton, NY 11973, USA*

¹⁶ *Department of Physics “E. Fermi”,
University of Pisa, I-56127, Pisa, Italy*

¹⁷ *University of Winnipeg, Winnipeg,
Manitoba R3T 2N2, Canada*

¹⁸ *Western Kentucky University,
Bowling Green, Kentucky, 42101, USA*

¹⁹ *Centre College, Danville, KY 40422, USA*

Recently, the $n^3\text{He}$ collaboration reported a measurement of the parity-violating (PV) proton directional asymmetry $A_{\text{PV}} = (1.55 \pm 0.97 \text{ (stat)} \pm 0.24 \text{ (sys)}) \times 10^{-8}$ in the capture reaction of ${}^3\text{He}(\vec{n}, p){}^3\text{H}$ at meV incident neutron energies. The result increased the limited inventory of precisely measured and calculable PV observables in few-body systems required to further understand the structure of hadronic weak interaction. In this letter, we report the experimental and theoretical investigation of a parity conserving (PC) asymmetry A_{PC} in the same reaction (the first ever measured PC observable at meV neutron energies). As a result of S- and P-wave mixing in the reaction, the A_{PC} is inversely proportional to the neutron wavelength λ . The experimental value is $(\lambda \times A_{\text{PC}}) \equiv \beta = (-1.97 \pm 0.28 \text{ (stat)} \pm 0.12 \text{ (sys)}) \times 10^{-6} \text{ \AA}$. We present results for a theoretical analysis of this reaction by solving the four-body scattering problem within the hyperspherical harmonic method. We find that in the ${}^3\text{He}(\vec{n}, p){}^3\text{H}$ reaction, A_{PC} depends critically on the energy and width of the close 0^- resonant state of ${}^4\text{He}$, resulting in a large sensitivity to the spin-orbit components of the nucleon-nucleon force and even to the three-nucleon force. The analysis of the accurately measured A_{PC} and A_{PV} using the same few-body theoretical models gives essential information needed to interpret the PV asymmetry in the ${}^3\text{He}(\vec{n}, p){}^3\text{H}$ reaction.

*Corresponding author, email: michele.viviani@pi.infn.it

Introduction. The study of polarization observables in nuclear reactions is an important tool - in some cases the only tool - to improve our understanding on issues ranging from fundamental symmetries to still ambiguous observations in the strong nuclear interaction. In this letter we present results from an investigation of the reaction of ${}^3\text{He}(\vec{n}, p){}^3\text{H}$ using transverse polarized cold neutrons (i.e. of meV energies) at the Spallation Neutron Source (SNS) of the Oak Ridge National Laboratory (ORNL). In a previous paper, we reported the parity-violating (PV) asymmetry $A_{\text{PV}} = (1.55 \pm 0.97 \text{ (stat)} \pm 0.24 \text{ (sys)}) \times 10^{-8}$ [1]. Here, we present the experimental and theoretical investigation of a parity-conserving (PC) asymmetry in the same reaction. In general, the cross section for ${}^3\text{He}(\vec{n}, p){}^3\text{H}$ can be written as

$$\frac{d\sigma}{d\Omega} = \left(\frac{d\sigma}{d\Omega} \right)_u \left(1 + A_{\text{PV}} \hat{s}_n \cdot \hat{k}_p + A_{\text{PC}} (\hat{s}_n \times \hat{k}_n) \cdot \hat{k}_p \right), \quad (1)$$

where $(d\sigma/d\Omega)_u$ is the unpolarized cross section and \hat{s}_n , \hat{k}_p , and \hat{k}_n denote unit vectors specifying the directions of the neutron polarization, the outgoing proton momentum, and the incoming neutron beam, respectively. The A_{PC} is measured by detecting emitted protons with their momenta in the plane defined by $\hat{s}_n \times \hat{k}_n$ and \hat{k}_n , and the A_{PV} in the plane \hat{s}_n and \hat{k}_n . The asymmetry is then deduced from detector yields with opposite neutron spin direction.

At a fundamental level, PV observables in nuclei are a consequence of the hadronic weak interaction (HWI) between quarks, which explains their very small values, see, for example, Ref. [2] for a recent review. Interest in measurements of A_{PV} in nucleon-nucleon (NN) systems (or in light nuclei) at low incoming neutron energies is therefore motivated by the effort to find additional insight to the structure of the HWI, the least-known part of the weak interaction [3–7]. Using the same beam and the A_{PV} experimental setup, the collaboration was able to measure A_{PC} , just by changing the plane of the detection of the emitted protons [1]. This is an important feature when systematic uncertainties are considered. As shown below, the observable is directly sensitive to the strong and electromagnetic components of the nuclear interaction, and contributions from the HWI can be safely neglected because they are estimated to be a few orders of magnitude smaller. Because A_{PC} is a consequence of the interference between S- and P-waves of the incoming neutron at meV energies, $A_{\text{PC}} \propto 1/\lambda$, where λ is the neutron wavelength. More specifically, the scale of the A_{PC} will be proportional to (kR) , where $k = 2\pi/\lambda$ and R a characteristic length for this reaction. For $\lambda = 5 \times 10^5$ fm, the neutron wave vector is $k \sim 1.3 \times 10^{-5} \text{ fm}^{-1}$ and using $R \sim 1.97$ fm for the ${}^3\text{He}$ radius, we obtain $(kR) \sim 2 \times 10^{-5}$. This is the expected order of magnitude of A_{PC} .

For the unpolarized ${}^3\text{He}(n, p){}^3\text{H}$ reaction, measurements of the total cross section and the differential cross

section exist at very low energies. No data for PC polarization observables were reported for this reaction, only for the mirror reaction ${}^3\text{H}(p, n){}^3\text{He}$ [8, 9]. These experiments were performed at proton incident energies corresponding to neutron energies of 300 keV or greater. Therefore, the measurement that we report here, is the first ever measurement of a PC ${}^3\text{He}(n, p){}^3\text{H}$ polarization observable at meV incident neutron energies.

Since the four-nucleon scattering problem can be routinely solved, A_{PC} can be accurately calculated starting from a given model of the strong and electromagnetic interactions [10–17]. This observable is usually very sensitive to the nuclear interaction, in particular, to spin-orbit components of the NN interaction and the three-nucleon (3N) force. This can be readily understood, since A_{PC} is a consequence of the interaction in P-waves. It is worth mentioning that in the physics of few-nucleon systems, we still have various discrepancies between theory and experiment, such as the famous “ A_y -puzzle” in $p-d$, $n-d$, and $p-{}^3\text{He}$ scattering [10, 18–22]. In the present case, this sensitivity could be amplified since the process under study is at an energy rather close to the energy of the second excited state of ${}^4\text{He}$, that has quantum numbers $J^\pi = 0^-$ [23]. Therefore, the study of this PC observable could be an extraordinary opportunity to study this poorly known resonance.

The energy spectrum of ${}^4\text{He}$ is, in fact, an important testing ground for understanding nuclear dynamics. Energies and widths of the various resonances have been determined in R-matrix analyses [23]. As a matter of fact, all excited states are resonances; however, their precise energies and widths contain critical information. Their calculation using different Hamiltonians gives slightly different results [9]. The first excited state, a 0^+ resonance, has been vigorously investigated both theoretically and experimentally. Without the Coulomb interaction, it would be a true bound state, with an energy well in agreement with that predicted in the framework of $A = 4$ Efimov physics [24]. This state has been studied experimentally by means of electron scattering, see Ref. [25] for a recent analysis. Theoretical studies have found that the position and width of this resonance are critically dependent on the interaction [26–30]. The next excited state, the 0^- resonance, is just above the threshold of $n-{}^3\text{He}$ dissociation, and has a similar width as the 0^+ resonance. Its existence is due to the interaction in P-waves.

Measurement and analysis of A_{PC} . The primary goal of the $n{}^3\text{He}$ experiment was a precision measurement of A_{PV} ; however, A_{PC} was also measured to support the theoretical analysis of the $n-{}^3\text{He}$ reaction and because it is a significant correction to A_{PV} , see Table 1 in Ref. [1]. To keep sources of systematic uncertainties in the A_{PC} and A_{PV} measurements comparable, the two measurements were designed so that the only change from the A_{PV} setup was a rotation of the target/detector cham-

ber around the beam axis by 90 degrees [1], to the most sensitive detector orientation for A_{PC} . We reported the uncorrected $A_{PC}^{unc} = (-41 \pm 5.6(\text{stat})) \times 10^{-8}$ in Ref. [1], extracted from the data with the same algorithm that was used for the A_{PV} data, where the asymmetry was calculated from integrating detector yields over a neutron wavelength range, 3.4–6.3 Å [1]. This averaging approach was possible in the case of the PV asymmetry, since it does not depend on incident neutron energy. However, A_{PC} has the $1/\lambda$ dependence that is incorporated to analysis of the A_{PC} data in this letter.

Corrections and systematic uncertainties for A_{PC}^{unc} are mainly due to the uncertainty in the chamber orientation. The first two corrections are produced by a twist of the signal wire frame stack in the detector [1] and then the alignment uncertainty of the spin holding magnetic field with the detector. These two alignment uncertainties mix the small PV value into the significantly larger PC value, and are therefore expected to be small. We get the frame twist and the field alignment correction to A_{PC}^{unc} to be -0.09 ± 0.00 ppb and 0.00 ± 0.04 ppb, respectively [1].

The origin of the third additive correction is the spin-orbit component of the electromagnetic neutron- ^3He atom interaction due to the Mott-Schwinger (MS) mechanism [31]. In fact, the probability that a neutron undergoes an elastic scattering on ^3He atoms in the target before being captured by another helium nucleus, is very small, $\sim 10^{-4}$, but, in any case, finite. This elastic scattering produces, via the MS mechanism, a small left-right asymmetry A_{MS} that is then “conserved” in the subsequent capture, which is essentially isotropic. The sequence (elastic scattering + capture) produces at the end a false asymmetry δA_{MS} , which has to be subtracted from A_{PC}^{unc} in order to obtain the PC asymmetry due solely to the capture process. We calculated A_{MS} following the approach described in Ref. [31]. Since it depends on the neutron wavelength λ , we have to average over the measured wavelength range at each wire plane j (the geometry of the detector chamber is briefly discussed in the caption of Fig. 1), i.e.

$$\bar{A}_{MS}^j = \int_{\lambda_{min}^j}^{\lambda_{max}^j} A_{MS}^j(\lambda) P^j(\lambda) d\lambda, \quad (2)$$

where $P^j(\lambda)$ is the yield density distribution of the wire plane. Fig. 1 shows yields from two central signal wires of the 1st and the 10th plane. The target chamber has total of 16 planes 19 mm apart. $\lambda_{min(max)}^j$ are the integration limits, unique in each wire plane due to the increasing distance of the planes from the moderator. The significant variation in the detector yield between the planes is due mainly to the large wavelength dependent n- ^3He capture cross section [32, 33] that exponentially decreases the beam intensity as it passes through the ^3He gas at a pressure of 43.6 kPa. The overall MS asymmetry \bar{A}_{MS} for the detector is obtained by calculating the average given

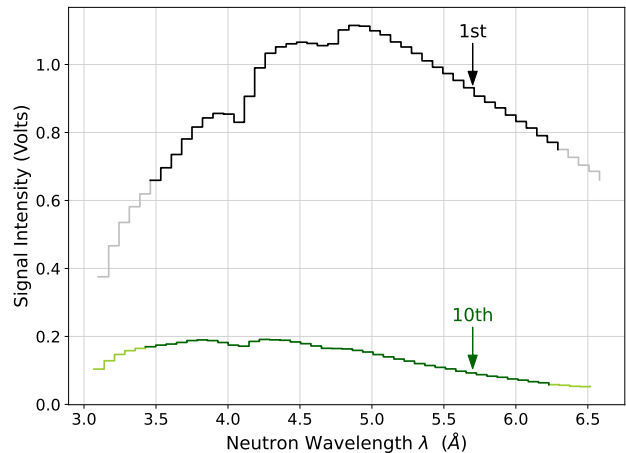


FIG. 1: The chamber has 16 signal wire planes. The measured outputs of the central signal wires of the 1st and the 10th wire plane have selected to indicate how the incoming neutron intensity and peak shape changes as the beam passes through the chamber. The signals were measured as a function of TOF but are plotted as a function of the neutron wavelength. The DAQ samples the wires at 20 μs intervals and then sums them into 49, 0.32 ms wide time bins. Due to 17 cm difference in distance between the two wire planes from the moderator, the neutron wavelengths on the 10th are little shorter than on the 1st wire, consequently, there is a half time bin shift between the wavelength plots. The signals represent collected charges after the $n^3\text{He}$ capture and the emitted proton and triton depositing their kinetic energy to ^3He gas at 43.6 kPa. The difference between the two spectra is mainly due to a large neutron energy dependent capture cross section on ^3He that reduces exponentially the intensity of the beam traveling down the chamber. For determination of β , see text for details, the integration is done over the same time bin range, meaning that each wire plane has a unique λ_{min} and λ_{max} for integration. The integration ranges of the two signals are indicated with thicker lines. The two small dips at 4.1 Å and 4.7 Å are residuals from neutron transmission Bragg-edges on Aluminum beamline windows.

in Eq. (2) for each of the 16 wire planes and then combining those using the integrated yield in the respective planes as the weighting factor. The final calculated value is $\bar{A}_{MS} = (-4.8 \pm 0.2) \times 10^{-5}$, that results in a correction $\delta \bar{A}_{MS} = (-1.36 \pm 0.07) \times 10^{-8}$ to A_{PC} . With the above corrections and those from Table 1 of Ref. [1], we obtain the final value for the measured PC asymmetry

$$A_{PC} = (-42.4 \pm 6.0(\text{stat}) \pm 0.23(\text{sys})) \times 10^{-8}, \quad (3)$$

where the error in the calculated value of $\delta \bar{A}_{MS}$ has been folded into the systematic uncertainty.

The incoming neutrons contributing to the PC asymmetry reported in Eq. (3), have a range of wavelengths. Since $A_{PC} \propto 1/\lambda$, we can write explicitly

$$A_{PC}(\mu) = \beta\mu, \quad (4)$$

where β is a constant that we want to extract from A_{PC} and $\mu = 1/\lambda$. The mean inverse wavelength over the integrated wave forms in each wire plane can be calculated as discussed previously in context of Eq. (2) and in the Appendix. For the overall $\bar{\mu}$ we obtain

$$\bar{\mu} = \left\langle \frac{1}{\lambda} \right\rangle = 0.2151 \pm 0.0015 \text{ \AA}^{-1}, \quad (5)$$

where the uncertainty is statistical, and is determined by the averaging process. With Eqs. (3)–(5), we get

$$\beta = (-1.97 \pm 0.28(\text{stat}) \pm 0.02(\text{sys})) \times 10^{-6} \text{ \AA}. \quad (6)$$

However, to finalize systematic uncertainty in β , we still need to work out the full uncertainties in $\bar{\mu}$.

In this pulsed neutron source, the wavelength of neutrons arriving at a detector location is calculated by the measured time of flight (*TOF*) over the known path length to that detector. In our case, the path length from the moderator emission surface to the 1st wire plane has been measured with relative accuracy of 0.2%. The *TOF* measurement is started by a clock signal corresponding to the arrival of the proton beam bunch on the mercury target to within 1 μs , the neutron emission time - a small correction to *TOF* due to time from start of *TOF* to moment when the neutron exits the moderator [34]. After a selected delay (13.500 ms), the DAQ system digitizes the signals in 49 time bins of 0.32 ms width. Fig. 1 shows typical yields, measured in the 1st and 10th wire planes as a function of *TOF* but presented as a function of wavelength. This presentation required that the plots had to be shifted little respect to the x-axis, since the two planes are at different distances from the moderator. The *TOF* calculation includes, as its most significant uncertainty, the uncertainty of the charge collection time, the time that is required to collect all the charges from the ionization by the emitted proton from the $n - ^3\text{He}$ capture. Results of Garfield++ simulations indicate that the collection time can be up to 1.5 ms long [35]. This is the dominating uncertainty in $\bar{\mu}$ and is carried over to the systematic uncertainty in β . A more detailed discussion of the determination of the uncertainty is contained in the Appendix. Our final result for β is

$$\beta = (-1.97 \pm 0.28 (\text{stat}) \pm 0.12 (\text{sys})) \times 10^{-6} \text{ \AA}. \quad (7)$$

Theoretical analysis. In the present paper the four-nucleon (4N) scattering problem is solved using the hyperspherical harmonics (HH) method [9, 37]. Here, we will give only some details of the procedure. First, a particular clusterization $A+B$ of the four-nucleon system in the asymptotic region is denoted with the index γ . More specifically, $\gamma = 1$ (2) corresponds to $p - ^3\text{H}$ ($n - ^3\text{He}$) clusterization. Consider a scattering state with total angular momentum quantum number JJ_z , and parity π . The asymptotic part of the wave function describing the

incoming clusters γ with relative orbital angular momentum L and total spin S (note that $\pi \equiv (-)^L$) is generally written as a sum of a (distorted) plane wave plus outgoing spherical waves in all possible channels γ', L', S' . The weights of the outgoing waves are the T-matrix elements (TMEs) ${}^J T_{LS, L'S'}^{\gamma, \gamma'}$. It is well known that ${}^J T_{LS, L'S'}^{\gamma, \gamma'} \sim q_2^L$ for $q_2 \rightarrow 0$ [9], where q_2 is the relative $n - ^3\text{He}$ momentum. To complete the calculation, the inner part of the wave function (where the nucleons are close between themselves) is described by an expansion over the HH basis (for more details, see Ref. [9]).

In terms of the TMEs, the transverse asymmetry can be written as

$$\begin{aligned} A_{\text{PC}} \sigma_0 = & 3\sqrt{2}\Im \left[({}^1 T_{11,10}^{2,1})^* {}^0 T_{00,00}^{2,1} \right] + 2\Im \left[({}^0 T_{11,11}^{2,1})^* {}^1 T_{01,01}^{2,1} \right] \\ & + 3\sqrt{2}\Im \left[({}^1 T_{10,11}^{2,1})^* {}^1 T_{01,01}^{2,1} \right] + 3\sqrt{2}\Im \left[({}^1 T_{11,11}^{2,1})^* {}^1 T_{01,01}^{2,1} \right] \\ & - 5\Im \left[({}^2 T_{11,11}^{2,1})^* {}^1 T_{01,01}^{2,1} \right], \end{aligned} \quad (8)$$

$$\sigma_0 = |{}^0 T_{00,00}^{2,1}|^2 + 3|{}^1 T_{01,01}^{2,1}|^2, \quad (9)$$

where in the expression of σ_0 we have retained only the contributions of S-wave TMEs (which are $\sim q_2^0$), and in A_{PC} the contribution of S- and P-waves. From the q_2 behavior discussed above, we see that $A_{\text{PC}} \sim q_2$. Note that $q_2 = (3/4)2\pi/\lambda$, hence $A_{\text{PC}} \sim 1/\lambda$ as discussed previously.

The A_{PC} observable has been obtained using the NN interaction derived by Entem and Machleidt at next-to-next-to-next-leading order (N3LO) in chiral effective field theory (EFT) [38, 39], corresponding to two different cutoff values ($\Lambda = 500$ MeV and $\Lambda = 600$ MeV). These NN interactions are labeled, respectively, N3LO500 and N3LO600. In this way, we can explore the dependence on the cutoff value Λ of the 4N observables. The 3N force considered here has been derived at next-to-next-leading order (N2LO) in Ref. [40] (the 3N force contributions at N3LO and beyond are still under construction but we plan to include them in future 4N calculations). With the N3LO500 (N3LO600) NN interaction, we have considered the 3N N2LO force, in the local coordinate space version [41], labeled N2LO500 (N2LO600) with the parameters c_D and c_E fixed to reproduce the 3N binding energy and the experimental Gamow-Teller (GT) matrix element and the tritium beta decay. The values of these parameters, recently redetermined in Ref. [42], are $(c_D, c_E) = (+0.945, -0.0410)$ for the N2LO500 force and $(c_D, c_E) = (+1.145, -0.6095)$ for the N2LO600 force.

In order to explore the dependence on the parameters c_D and c_E , we use also another 3N N2LO force labeled N2LO500*. In this case, the interaction reproduces the 3N binding energies but not the tritium GT matrix element. The corresponding values of the parameters are chosen arbitrarily to be $(c_D, c_E) = (-0.12, -0.196)$.

We also report results obtained using the Norfolk NN interactions, also derived within chiral EFT, but using as degrees of freedom nucleons, pions and Δ s [43, 44]. In this case, the potentials are regularized in coordinate space. We use the so-called NVIa and NVIb NN interactions, regularized with cutoff $R_L = 1.2$ and 1.0 fm, respectively. They are augmented by 3N N2LO interactions, with $(c_D, c_E) = (-0.635, -0.090)$ for the NVIa force and $(c_D, c_E) = (-4.71, +0.55)$ for the NVIb force (see Table IV of Ref. [45]).

In all cases, the electromagnetic force between the nucleons has been approximated by the point-Coulomb potential. Effects due to other terms, as the magnetic dipole interaction, the vacuum polarization term, etc. are thought to be very small in capture observables.

For each interaction, the convergence of the calculated TMEs has been checked by increasing the size of the HH basis. The only problematic quantity to be calculated has been found to be the 0^- TME, due to the difficulty of constructing the 4N wave function close to the 0^- resonance.

In order to explore the properties of this resonance, we have performed a series of calculations for different neutron energies. From the TMEs we can extract also the resonance position E_R and width Γ , using the procedure described in Ref. [9]. Results are reported in columns 2 and 3 of Table I. The values are generally smaller than those extracted from the experiment using an R-matrix analysis [23] (actually, the two methods do not necessarily give the same result). The E_R value in correspondence with the N3LO500/N2LO500 interaction is found to be smaller than for the other cases. Also the width Γ is found to be narrower.

We note that A_{PC} is very sensitive to the value of ${}^0t_{11,11}^{2,1} = \lim_{q_2 \rightarrow 0} |{}^0T_{11,11}^{2,1}|/q_2$, reported in the 4th column of the table. Note the large variation with the different interactions. Tiny differences of the position of the 0^- resonance reflect in large changes in ${}^0t_{11,11}^{2,1}$.

Finally, in column 5 we report the calculated values of $\beta = A_{PC} \times \lambda$ for the various interactions using Eq. (8). The calculations have been performed at $q_2 = 0$ (namely, at $\lambda \rightarrow \infty$), but in any case, for these energies β is independent of q_2 . The large differences between the results for β reflect the fact that the various terms in Eq. (8) tend to cancel each other, in particular the first two, which are the largest ones. Furthermore, note that without the contribution of the ${}^0T_{11,11}^{2,1}$ term, A_{PC} would be positive, at variance with what found experimentally. The A_{PC} with N3LO500/N2LO500 is found to be too large (in absolute value), due to the large value of ${}^0T_{11,11}^{2,1}/q_2$. This is probably a consequence of the fact that for this interaction the 0^- resonance is very close to the $n - {}^3\text{He}$ threshold.

The interaction N3LO500/N2LO500* differs from N3LO500/N2LO500 just for c_D, c_E values. In this case A_{PC} is found to be in good agreement with the experimental value. This result shows the sensitivity of this ob-

TABLE I: Results of the calculations performed using the HH method. In columns 2 and 3, we report the position E_R and width Γ of the ${}^4\text{He}$ 0^- resonance obtained as discussed in Ref. [9]. Note that E_R is calculated starting from the $n - {}^3\text{He}$ threshold (nearly 20.58 MeV above the ${}^4\text{He}$ ground state energy). In column 4, we report the values of ${}^0t_{11,11}^{2,1} = \lim_{q_2 \rightarrow 0} |{}^0T_{11,11}^{2,1}|/q_2$ and in column 5 the quantity β as defined in Eq. (4) (we remember that this quantity at low energies is independent of q_2). In the last row, we report the experimental values for E_R, Γ [23], and β , the latter quantity obtained as discussed in the main text.

Interaction	E_R [MeV]	Γ [MeV]	${}^0t_{11,11}^{2,1}$ [fm]	$\beta \times 10^6$ [Å]
N3LO500	0.16	0.41	20.7	-4.83
N3LO600	0.24	0.51	16.9	-2.68
NVIa	0.31	0.53	17.3	-2.61
NVIb	0.30	0.54	13.0	-0.43
N3LO500/N2LO500	0.06	0.26	30.1	-10.04
N3LO500/N2LO500*	0.14	0.41	18.5	-2.68
N3LO600/N2LO600	0.09	0.30	25.9	-5.28
NVIa/3N	0.04	0.36	35.4	-12.17
NVIb/3N	0.12	0.40	23.9	-5.15
Experimental	0.44	0.84		-1.97 ± 0.28 (stat) ± 0.12 (sys)

servable to the details of the 3N force. The difference between the N3LO500/N2LO500 and N3LO600/N2LO600 results shows the sensitivity of this observable to the cutoff values and consequently to the different treatment of the short-range physics.

Conclusions. The first accurate measurement of a parity-conserving proton directional asymmetry at reaction of ${}^3\text{He}(\vec{n}, p){}^3\text{H}$ at meV incident neutron energies resulted in $A_{PC} = (-42.4 \pm 6.0(\text{stat}) \pm 0.23(\text{sys})) \times 10^{-8}$. Since the A_{PC} depends on $1/\lambda$, where λ is neutron wavelength, we can remove the λ dependence and obtain a constant $\beta = (\lambda \times A_{PC}) = (-1.97 \pm 0.28(\text{stat}) \pm 0.12(\text{sys})) \times 10^{-6}$ Å. In this reaction, A_{PC} comes out from the S- and P-wave interference induced mainly by the strong nuclear interaction. The difference between the final A_{PC} and the uncorrected A_{PC}^{unc} [1] is only 3%; this small improvement in the A_{PC} does not cause any significant corrections to the published $A_{PV} = (1.55 \pm 0.97(\text{stat}) \pm 0.24(\text{sys})) \times 10^{-8}$ [1].

This accurate measurement of the A_{PC} represents an important testing ground for nuclear physics studies, in particular those involving polarized neutrons. We have calculated A_{PC} using a number of modern nuclear interactions derived in the framework of chiral EFT. We have found that this observable depends critically on the 0^- TME. This quantity is in turn very sensitive to the nuclear Hamiltonian, since the experiment is performed at

an energy close to a rather sharp 0^- resonance in the ^4He spectrum. Thus, this observable works like a magnifying glass for the nuclear dynamics, and in particular for NN P-wave and 3N interactions, so that this study can give valuable information on these small components of the interaction and can be very useful in order to construct more accurate nuclear potentials. This can have a noticeable impact on other studies where the accurate determination of the nuclear matrix elements is crucial, as, for instance, in the case of the neutrinoless double beta decay.

Finally, we comment on the impact of this study on the PV observable A_{PV} . As we have seen, the difficulty in the prediction of A_{PC} is due to the large variability in the TME ${}^0T_{11,11}^{2,1}$. However, this element does not enter in the calculation of A_{PV} (it is suppressed with respect to other terms by a factor $\sim q_2$). Therefore, the theoretical prediction of A_{PV} is much less sensitive to the choice of the strong Hamiltonian.

Appendix: The ${}^3\text{He}(\bar{n}, p){}^3\text{H}$ parity-conserving asymmetry

Here, we give a more detailed discussion on the ion and the electron collection in the chamber and how it defines the main systematic uncertainty in the inverse neutron wavelength $\bar{\mu}$. The charge collection process is studied by performing Garfield++ simulations in a chamber model [35]. After determining the final systematic uncertainty in $\bar{\mu}$, we calculate the $\beta = A_{\text{PC}}/\bar{\mu}$ and its value is finally given in Eq. (7) of the paper.

Fig. 2 shows a cross sectional view of the truncated chamber model used to study charge collection and crosstalk between wire cells. For charge collection the ${}^3\text{He}^+$ ion and electron pairs are produced on each start point along the diagonal dotted line. Then Garfield++ calculates the time it takes for ions to reach high voltage wires or for electrons to collect onto signal wires [35]. The drift velocities of the ions and the electrons in the chamber are defined by the ${}^3\text{He}$ number density and the local electrical field strength produced by -350 V [35].

Fig. 3 shows the calculated average ${}^3\text{He}^+$ collection times with standard deviation in the wire cells as a function of initial location of ion production on the dotted line. The created ions are drifting towards HV wires driven by strength of the local electrical fields and collisions with ${}^3\text{He}$ atoms in gas. The ion collection times in the simulated geometry can extend up to 1.1 ms. The Garfield++ results for the electron drifting times have the same shape as ions, but the maxima are on the signal wires and the average collection times are three orders of magnitude shorter than for ions [35]. Depending on the location of the start of the ion-electron pair in the chamber, Garfield++ simulations result in the collection times that can be up to 1.8 ms long [35]. When estimating uncertainties in neutron wavelength (or inverse wavelength) calculations, the 1.8 ms ion collection time dominates all the other *TOF* uncertainties, i.e. the electron collection

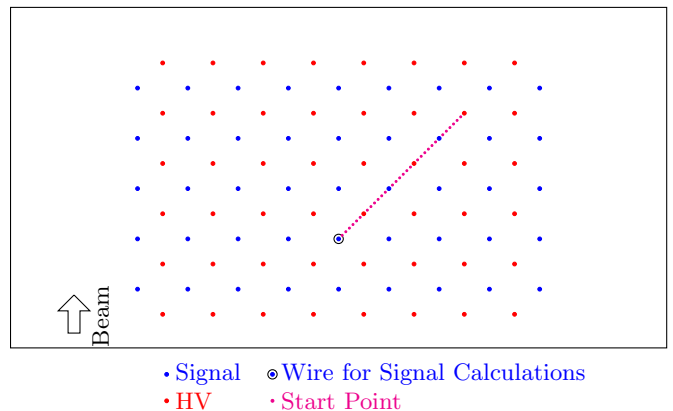


FIG. 2: A geometry for the charge collection Garfield++ simulations that is discussed in text. Shown is a scaled cross section of the truncated target chamber model, where signal (blue) and HV (red) wires are perpendicular to the page. The black outline is the grounded surface corresponding to the inside face of the cylindrical target vessel. The wire separation and housing are to scale. The distance between signal (or HV) wire planes is 1.9 cm. Ion-electron pairs are created on each of the 35 start points of the upwards going diagonal dotted line. Garfield++ transports the released charges at ${}^3\text{He}$ pressure of 43.6 kPa and in electrical field produced by -350 V on HV wires and calculates induced signals on the indicated wires and average drifting times to reach either a HV or a signal wire.

times, the 0.32 ms width of the DAQ time bin and the 0.140 ms FWHM of the emission time distribution from moderator for neutrons with same energy [34].

From distribution of charge collection times, it can be estimated that about 70 % of ions are collected at about 0.8 ms, and since the electron collection times are much shorter, the 0.8 ms time is used as a charge collection time uncertainty in *TOF*. Adding the *TOF* uncertainties - 0.8 ms, 0.32 ms and 0.140 ms - in quadrature, we obtain that the error due to *TOF* is ± 0.87 ms.

The neutron wavelength is calculated using the relation

$$\lambda = \frac{\hbar}{mv} = \frac{\hbar t}{ml}, \quad (10)$$

where m is the neutron mass, l is the neutron path length, i.e. the distance from the moderator surface to a wire plane in the chamber. This distance is known accurately through surveys. Furthermore, t is the neutron *TOF*, i.e. the time it takes the neutron travel to length l . As explained in the paper, the *TOF* measurement starts when the proton beam interacts with the mercury target. Therefore, the *TOF* has to be corrected with the neutron emission time (0.07 ms, with a weak neutron energy dependence), a time from start of *TOF* to moment when the neutron exits the moderator [34]. Because of the slow speed of the neutrons and the long distance to detector (17 m), the start of the DAQ measurement has to be delayed by 13.500 ms to sample the wavelength

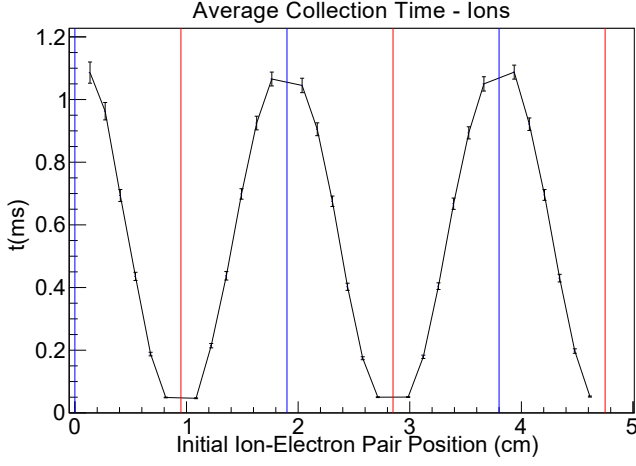


FIG. 3: The average ${}^3\text{He}^+$ -ion collection times with the geometry of Fig. 2. The vertical blue and red lines indicate the locations of signal and HV wires. Collection times are shown for each ion created on 35 dots of the source line with standard deviation. Drift times depend on distance to wire and strength of varying electrical field. Ion-Electron pair position is the horizontal displacement relative to the Wire for Signal Calculations marked in figure 2. The line connecting the points is just for guiding purpose.

range of interest. The *TOF* measurement ends when the neutron reaches the wire. The DAQ digitizes the signals in 49 time bins of 0.32 ms width.

Since the measured A_{PC} is an average value over the range of wavelengths and $A_{\text{PC}} \propto 1/\bar{\lambda}$, then $A_{\text{PC}}(\mu) = \beta \times \bar{\mu}$, where β is a constant that we want to extract from A_{PC} and $\bar{\mu} \equiv 1/\bar{\lambda}$.

Next, we determine the weighted average of the neutron wavelength and the inverse wavelength in the integration time window used for the asymmetry calculation without including uncertainties in the distances or in the *TOF*. The weighted average wavelength calculated for each of the 16 wire planes j by integrating over 40 time bins i in each plane is

$$\bar{\lambda}^j = \frac{\sum_i \lambda_i^j P_i^j}{\sum_i P_i^j}, \quad (11)$$

where $\bar{\lambda}_i^j$ is calculated by substituting in Eq. (1) l with the distance from the moderator surface to the wire plane j and $t = \text{TOF} = (13.500 - 0.07)$ ms, the time when DAQ starts sampling. The distance between wire planes is 1.9 cm. P_i^j is the measured detector yield distribution in each time bin i of the center wire of the plane j . To obtain the overall mean wavelength of the chamber, the mean wavelengths of the 16 planes are combined in a weighted mean, where the weighting factor is the yield of the central wire of the plane integrated over the time bin window.

The mean inverse wavelength of the chamber $\bar{\mu}$, is obtained by replacing variable λ_i^j in Eq. (2) with $1/\lambda_i^j$ and

then repeating the process performed for $\bar{\lambda}$.

For the detector yield weighted mean neutron wavelength and inverse wavelength across 16 wire planes we obtain

$$\bar{\lambda} = 4.7775 \pm 0.0317 \text{ \AA} \quad \text{and} \quad (12)$$

$$\bar{\mu} = 0.2152 \pm 0.0015 \text{ \AA}^{-1}, \quad (13)$$

where errors are statistical.

Finally, we set the upper and lower systematic limits to $\bar{\lambda}$ and $\bar{\mu}$, which then determines limits for β . The Q -value of the neutron- ${}^3\text{He}$ capture is 765 keV, that is shared as a kinetic energy between the final state proton, 571 keV, and the triton, 194 keV. At 43.6 kPa pressure of ${}^3\text{He}$ the proton from the decay can travel up to 14 cm [35]. An uncertainty in the neutron path length can be selected to be ± 14 cm, which is close to 1% uncertainty in the neutron path length, and the *TOF* uncertainty of ± 0.87 ms is used. With these systematic uncertainties we calculate the weighted average upper and lower limits to $\bar{\lambda}$ across the 16 wire planes with the process described above. As a result we obtain

$$\bar{\lambda} = 4.78 \pm 0.03 \text{ \AA}, \quad (14)$$

$$\lambda_{\text{max}} = 5.01 \pm 0.03 \text{ \AA}, \quad (15)$$

$$\lambda_{\text{min}} = 4.74 \pm 0.03 \text{ \AA}. \quad (16)$$

Correspondingly, the weighted average inverse wavelength $\bar{\mu}$ for the integrated time bins in each wire plane is calculated to be

$$\bar{\mu} = 0.2151 \pm 0.0015 \text{ \AA}^{-1}, \quad (17)$$

$$\mu_{\text{min}} = 0.2046 \pm 0.0014 \text{ \AA}^{-1}, \quad (18)$$

$$\mu_{\text{max}} = 0.2169 \pm 0.0015 \text{ \AA}^{-1}. \quad (19)$$

With $\bar{\mu}$ from Eq.(8) and A_{PC} from Eq. (3) of the paper, we can extract the central value for β ,

$$\beta = A_{\text{PC}}/\bar{\mu}, \quad (20)$$

$$= [-1.972 \pm 0.28(\text{stat}) \pm 0.017(\text{sys})] \times 10^{-6} \text{ \AA}^{-1}, \quad (21)$$

while for the upper and lower limits in β we get

$$\beta_{\text{min}} = [-0.2074 + / - 0.0279] \times 10^{-6} \text{ \AA}^{-1}, \quad (22)$$

$$\beta_{\text{max}} = [-0.1956 + / - 0.0279] \times 10^{-6} \text{ \AA}^{-1}. \quad (23)$$

The difference between the minimal and maximal values of β is then used to set a stronger systematic uncertainty in β ,

$$\Delta\beta = |\beta_{\text{max}} - \beta_{\text{min}}| \quad (24)$$

$$= 0.1179 \times 10^{-6} \text{ \AA}^{-1}. \quad (25)$$

Combining the systematic uncertainties of Eqs (12) and (16) in quadrature, we obtain the final uncertainty for β of 0.119×10^{-6} . This gives the final β -value of

$$\beta = [-1.97 \pm 0.28(\text{stat}) \pm 0.12(\text{sys})] \times 10^{-6} \text{ \AA}^{-1}. \quad (26)$$

Acknowledgements We gratefully acknowledge the support of the U.S. Department of Energy Office of Nuclear Physics through grant No. DE-FG02-03ER41258, DE-AC05-00OR22725, DE-SC0008107 and DE-SC0014622, the US National Science Foundation award No: PHY-0855584, the Natural Sciences and Engineering Research Council of Canada (NSERC), the Canadian Foundation for Innovation (CFI), and the Mexican PAPIIT-UNAM award No. IN11913 and AG102023. This research used resources of the SNS of ORNL, a DOE Office of Science User Facility.

-
- [1] M.T. Gericke *et al.* (The n3He Collaboration), Phys. Rev. Lett. **125**, 131803 (2020).
- [2] J. de Vries, E. Epelbaum, L. Girlanda, A. Gnech, E. Mereghetti, and M. Viviani, Frontiers in Physics **8**, 218 (2020).
- [3] M.J. Ramsey-Musolf and S.A. Page, Ann. Rev. Nucl. Part. Sci. **56**, 1 (2006).
- [4] W.C. Haxton and B.R. Holstein, Prog. Part. Nucl. Phys., **71**, 185 (2013).
- [5] M.R. Schindler and R.P. Springer, Prog. Part. Nucl. Phys., **72**, 1 (2013).
- [6] B. Desplanques, J.F. Donoghue, and B.R. Holstein, Ann. Phys. (N.Y.) **124**, 449 (1980).
- [7] D.B. Kaplan and M.J. Savage, Nucl. Phys. A **556**, 653 (1993); Erratum *ibid.* A **570**, 833 (1994); Erratum *ibid.* A **580**, 679 (1994).
- [8] See, for example, <https://www-nds.iaea.org/exfor/>
- [9] M. Viviani, L. Girlanda, A. Kievsky, and L.E. Marcucci, Phys. Rev. C **102**, 034007 (2020).
- [10] A. Deltuva and A.C. Fonseca, Phys. Rev. C **75**, 014005 (2007); Phys. Rev. Lett. **98**, 162502 (2007); Phys. Rev. C **76**, 021001(R) (2007).
- [11] A. Deltuva and A.C. Fonseca, Phys. Rev. C **95**, 024003 (2017).
- [12] R. Lazauskas, Phys. Rev. C **79**, 054007 (2009).
- [13] R. Lazauskas and J. Carbonell, Frontiers in Physics **7**, 251 (2020).
- [14] B. Pfitzinger, H.M. Hofmann, and G.M. Hale, Phys. Rev. C **64**, 044003 (2001).
- [15] P. Navrátil, R. Roth, and S. Quaglioni, Phys. Rev. C **82**, 034609 (2010).
- [16] S. Aoyama, K. Arai, Y. Suzuki, P. Descouvemont, and D. Baye, Few-Body Syst. **52**, 97 (2012).
- [17] M. Viviani, A. Deltuva, R. Lazauskas, A.C. Fonseca, A. Kievsky, and L.E. Marcucci, Phys. Rev. C **95**, 034003 (2017).
- [18] Y. Koike and J. Haidenbauer, Nucl. Phys. **A463**, 365c (1987).
- [19] H. Witala, W. Glöckle, and T. Cornelius, Nucl. Phys. **A491**, 157 (1988).
- [20] A. Kievsky *et al.*, Nucl. Phys. **A607**, 402 (1996).
- [21] A.C. Fonseca, Phys. Rev. Lett. **83**, 4021 (1999).
- [22] M. Viviani, L. Girlanda, A. Kievsky, and L.E. Marcucci, Phys. Rev. Lett. **111**, 172302 (2013).
- [23] D.R. Tilley, H.R. Weller, and G.M. Hale, Nucl. Phys. A **541**, 1 (1992).
- [24] A. Kievsky, L. Girlanda, M. Gattobigio, and M. Viviani, Ann. Rev. Nucl. Part. Sci. **71**, 465 (2021).
- [25] S. Kegel *et al.*, [arXiv:2112.10582](https://arxiv.org/abs/2112.10582).
- [26] E. Hiyama, B.F. Gibson, and M. Kamimura, Phys. Rev. C **70**, 031001(R) (2004).
- [27] S. Bacca, N. Barnea, W. Leidemann, and G. Orlandini, Phys. Rev. Lett. **110**, 042503 (2013).
- [28] S. Bacca, N. Barnea, W. Leidemann, and G. Orlandini, Phys. Rev. C **91**, 024303 (2015).
- [29] N. Michel, W. Nazarewicz, and M. Płoszajczak, [arXiv:2306.05192](https://arxiv.org/abs/2306.05192)
- [30] Ulf-G. Meißner, S. Shen, S. Elhatisari, and D. Lee, [arXiv:2309.01558](https://arxiv.org/abs/2309.01558)
- [31] M.T. Gericke, J.D. Bowman, and M.B. Johnson, Phys. Rev. C **78**, 044003 (2008).
- [32] Neutron News, Vol. 3, No. 3, 29, (1992). <http://www.ncnr.nist.gov/resources/n-lengths/>.
- [33] J. Als-Nielsen and O. Dietrich, Phys. Rev. **133**, B925 (1964). <https://doi.org/10.1103/PhysRev.133.B925>.
- [34] W. Lu, SNS-106100200-TR0199-R00, 2013.
- [35] M. McCrea, PhD Thesis, University of Manitoba, Winnipeg (Canada) (2016).
- [36] Ramadhan, R.S. *et al.*, J. Appl. Cryst. (2019). 52, 351-368. <https://doi.org/10.1107/S1600576719001730>
- [37] L.E. Marcucci, J. Dohet-Eraly, L. Girlanda, A. Gnech, A. Kievsky, and M. Viviani, Frontiers in Physics **8**, 69 (2020).
- [38] D.R. Entem and R. Machleidt, Phys. Rev. C **68**, 041001(R) (2003).
- [39] R. Machleidt and D.R. Entem, Phys. Rep. **503**, 1 (2011).
- [40] E. Epelbaum *et al.*, Phys. Rev. C **66**, 064001 (2002).
- [41] P. Navrátil, Few-Body Syst. **41**, 117 (2007).
- [42] L.E. Marcucci, A. Kievsky, S. Rosati, R. Schiavilla, and M. Viviani, Phys. Rev. Lett. **121**, 049901(E) (2018).
- [43] M. Piarulli *et al.*, Phys. Rev. C **94**, 054007 (2016).
- [44] M. Piarulli *et al.*, Phys. Rev. Lett. **120**, 052503 (2017).
- [45] A. Baroni *et al.*, Phys. Rev. C **98**, 044003 (2018).